Journal of Quantitative Spectroscopy & Radiative Transfer 248 (2020) 106961

Contents lists available at ScienceDirect

Journal of Quantitative Spectroscopy & Radiative Transfer

journal homepage: www.elsevier.com/locate/jqsrt

Mode coupling in arrays of Al nanoparticles

Alexander E. Ershov[a,b], Valeriy S. Gerasimov[a,b,*], Rashid G. Bikbaev[c,b], Sergey P. Polyutov[b], Sergey V. Karpov[c,b,d]

[a] Institute of Computational Modeling SB RAS, Krasnoyarsk, 660036, Russia
[b] Siberian Federal University, Krasnoyarsk, 660041, Russia
[c] L.V. Kirensky Institute of Physics, Federal Research Center KSC SB RAS, Krasnoyarsk, 660036, Russia
[d] Siberian State University of Science and Technology, Krasnoyarsk 660014, Russia

ARTICLE INFO

Article history:
Received 31 January 2020
Revised 12 March 2020
Accepted 12 March 2020
Available online 21 March 2020

Keywords:
Plasmonics
Aluminum
Surface lattice resonances

ABSTRACT

The mechanisms of coupling between the lattice modes of a two-dimensional (2D) array consisting of Al nanoparticles and the localized modes of individual Al nanoparticles have been studied in detail. The results were obtained employing the finite-difference time-domain method (FDTD) and the generalized Mie theory. It was shown that interactions of single particles with 2D lattice modes significantly change the extinction spectra depending on the particle radius and the lattice period. The Rayleigh anomalies of higher orders contribute to formation of hybrid modes resulting in increase of the extinction efficiency in short wavelength range of the spectrum. It was shown that high intensity magnetic modes are excited in aluminum nanoparticles arrays. The patterns of spatial electromagnetic field distribution at the frequencies of hybrid modes have been studied. We note that comprehensive understanding the mode coupling mechanisms in arrays paves the way for engineering different types of modern photonic devices with controllable optical properties.

1. Introduction

It is generally known that emergence of electromagnetic modes of different orders is possible in the process of interaction of optical radiation with single isolated nanoparticles as well as with their groups. For spherical particles the first-order modes are electro- and magneto-dipole ones [1]. The excitation of higher order modes can be achieved by increase of the particles size and by the shape of the incident wave front. In the case of an periodic structures (e.g. nanoparticle lattices) the interaction of the local modes of each individual particle with the collective resonances was mentioned in early works by Rayleigh [2] and Wood [3]. The emergence of these resonances in periodic arrays of plasmonic nanoparticles has been predicted in Refs [4–6] and experimentally demonstrated in Refs. [7–9]. Later these collective lattice resonances were studied in a wide range of periodic nanostructures with different types of unit cells: single [10,11] or paired (in a stack) [12] nanodisks, the cylinders with the core-shell structure [13], dimers [14,15], and more complicated configurations [16–20].

Such structures have found wide applications in many areas, e.g. in IR spectroscopy [21], narrow-band light absorption [22], sensorics [23,24], lasers [25] and enhanced fluorescence [26,27], just to name a few. It is known that silver and gold are the best plasmonic materials, but in recent years the attention was attracted to alternative plasmonic materials such as transparent conductive oxides (AZO, GZO, ITO) [28] and titanium nitride (TiN) which made it possible to obtain high-Q collective modes (up to $Q = 10^4$) in the telecommunication spectral range [29].

Aluminum plasmonics appeared quite recently [30,31] and interest in this material was associated with a high value of the plasma frequency – much higher than that of silver or gold, which made it possible to observe surface plasmon resonances in the ultraviolet (UV) spectral range. This feature would find application, for example, in photocatalysis and for studying of organic and biological systems that exhibit strong UV absorption [32–34]. The interest to aluminum in that respect is aroused also due to its relative cheapness and availability that opens wide opportunities for manufacturing and mass production in such promising areas as color printing [35–37], photovoltaics [38–41], thermoplasmonics [42], holography [43]. The plasmonic properties of Al structures were extensively studied in numerous papers: single nanoparticles with various shapes [30,44–50], dimers [51], heterodimers [52], and large arrays [10,53]. Surface lattice resonances (SLRs) with ac-

* Corresponding author at: Institute of Computational Modeling SB RAS, Akademgorodok 50, bld#.44, Krasnoyarsk 660036, Russian Federation.
E-mail address: gerasimov@icm.krasn.ru (V.S. Gerasimov).

https://doi.org/10.1016/j.jqsrt.2020.106961
0022-4073/

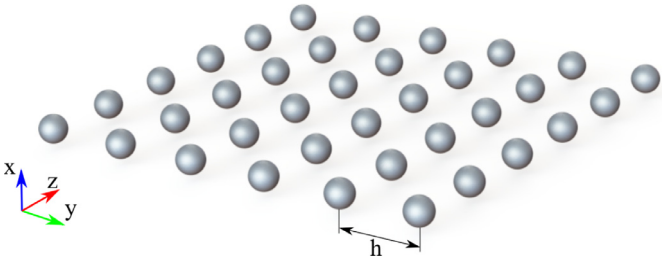

Fig. 1. Sketch view of the square Al nanoparticles array.

tive tuning [54,55] has been shown to cover wide range of frequencies in Al and used for nonlinear optics [56], lasers [57–59], temperature sensing [60], photoluminescence [43,61–63], light emission [64] and confinement [65], quantum electrodynamics [66], sensor on Al metal film holes [67]. The multipoles in single Al nanoparticle are studied in Ref. [68]. The methods for synthesis can be found in Ref. [69], while the methods to decrease the losses in Al nanoparticles are described in Ref. [70].

Obviously that practical implementation and engineering of devices based on periodic arrays requires the understanding both how the modes of individual particles in the array interact with the lattice modes and how to control the hybrid modes.

The goal of our paper is the studying of interaction of local modes (both electric and magnetic ones) of individual particles with the collective modes of nanoparticle periodic arrays. It covers the optical properties of hybrid modes for different nanoparticle radii and lattice periods investigated by analytically accurate generalized Mie theory and commercial FDTD package (Finite-Difference Time-Domain Method). This makes it possible to determine the contribution of each partial hybrid mode to the extinction spectra and to control the extinction spectra of the structure as a whole.

2. Computational model

2.1. The array structure

Schematic representation of the structure used in our simulations is shown in Fig. 1: regular square 2D array of aluminum nanospheres with radius R and period h along x and y axis, respectively, is immersed in the dielectric media with permittivity $\varepsilon_m = 2.25$ (optical glass) and we used tabulated values of dielectric constants ε of aluminum [71] in simulations.

2.2. Definition of the extinction

In this paper we consider the extinction spectra of both single nanoparticles and periodic arrays (finite and infinite) using generalized Mie theory and Finite-Difference Time-Domain (FDTD) method. Importantly, that the definitions of scattering, extinction and transmission cross-sections either for finite or infinite periodic structures are different.

In the case of infinite structures the following definition of extinction, scattering, and transmission is commonly used. Namely, the transmission cross-section is determined by the power of the electromagnetic field (relative to the intensity of the incident radiation) that passed through the periodic structure and the sum of scattering and absorption cross-sections corresponds to the residual power of the electromagnetic field.

The case of finite structures is different in comparison with the one of infinite structures and there is the following definition. Note, that electromagnetic field outside the particles (**E, H**) can be considered as the sum of incident and scattered ones. So, the scattered field can be considered as the difference between full (**E, H**) and incident fields.

$$\begin{aligned} \mathbf{E}_{sca} &= \mathbf{E} - \mathbf{E}_i, \\ \mathbf{H}_{sca} &= \mathbf{H} - \mathbf{H}_i. \end{aligned} \tag{1}$$

Here $\mathbf{E}_i$ and $\mathbf{H}_i$ are the components of incident electromagnetic field which define the electromagnetic field in the interparticle medium in the absence of the particles. In this case the scattering cross-section is determined by the power of the fields ($\mathbf{E}_{sca}$, $\mathbf{H}_{sca}$).

It is clear that for correct comparison of finite and infinite structures spectra one should choose either one or another approach mentioned above and apply it to the both types of structures.

The first definition is not generally applicable to finite structures without introducing additional conventions (for example, introducing a structure plane for a single particle by analogy with the plane of the array).

The second definition can be applied to the both — infinite and finite structures. Therefore, it was chosen as the definition of extinction in all our simulations. However, for infinite structures, this method has an important feature which should be taken into account: the extinction efficiency can exceed an unity that gives incorrect impressions of either incorrect definition, or a violation of the energy conservation law. It is clear that the amplitude of the far-field (**E, H**) will not exceed the amplitude of the incident field, but we should note that the fields (**E, H**) and ($\mathbf{E}_i$, $\mathbf{H}_i$) may have different phases. This means that the interference effects can lead to the dominance of the scattering field in Eq. (1) over the incident field resulting in rising of the extinction efficiency. As mentioned in the paper by V. A. Markel [72], only the absorbed energy is defined in terms of a physical energy flux, that is, a flux that actually exists in space. The scattered energy is defined in terms of the flux that is created by the scattered field alone. The extinction power is defined in terms of a peculiar flux that is created by the interference between the incident and the scattered fields.

2.3. Finite-difference time-domain method

To calculate extinction spectra of infinite nanosphere arrays commercial FDTD package was employed [73]. Total field scattered field (**TFSF**) radiation source (see [74]) was applied to separate the incident electromagnetic field ($\mathbf{E}_i$, $\mathbf{H}_i$) which is defined as the electromagnetic field in the interparticle medium in the absence of the particles and the scattered electromagnetic field ($\mathbf{E}_{sca}$, $\mathbf{H}_{sca}$) that made it possible to find extinction and scattering cross-sections (σ_{ext}, σ_{sca}).

The array was illuminated from the top by the plane wave with normal incidence along x axis and polarization along y axis. Absorption Q_{abs} has been calculated using a set of monitors surrounding NP. The scattering efficiency Q_{sca} has been calculated as the sum of two monitors placed outside TFSF region before and after the structure. The extinction efficiency (eq. 7) we define as $Q_{ext} = Q_{abs} + Q_{sca}$. Periodic boundary conditions have been applied at the lateral boundaries of the simulation box, while perfectly matched layer (PML) boundary conditions were used on the remaining top and bottom sides. An adaptive mesh has been used to reproduce accurately the nanosphere shape.

2.4. Generalized Mie theory

The generalized Mie theory [75] allows to calculate the extinction, scattering, and absorption spectra of spherical nanoparticles system. The incident and scattering coefficients are given by the

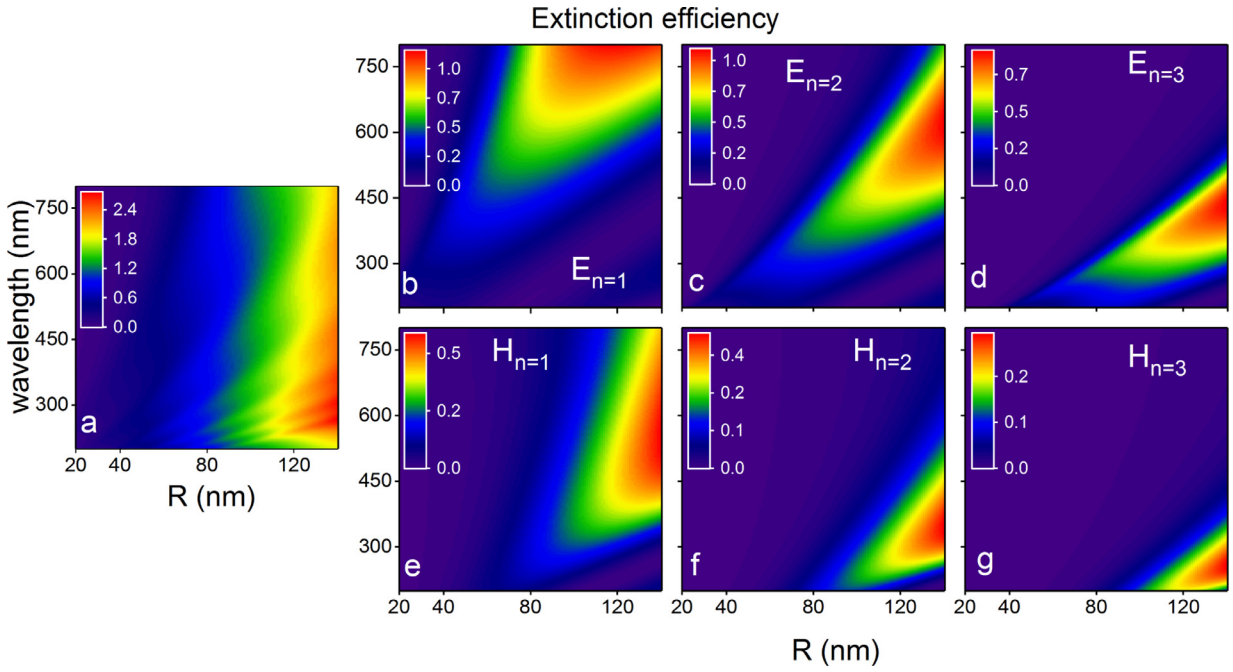

Fig. 2. Extinction efficiency decomposed in a set of spherical multipoles for single aluminum nanospheres of different radii R and wavelengths of incident light.

equations

$$a_{mn}^{j} = \frac{(m^j)^2 j_n(m^j x^j)\left(x^j j_n(x^j)\right)' - j_n(x^j)\left(m^j x^j j_n(m^j x^j)\right)'}{(m^j)^2 j_n(m^j x^j)\left(x^j h_n^{(1)}(x^j)\right)' - h_n^{(1)}(x^j)\left(m^j x^j j_n(m^j x^j)\right)'} p_{mn}^{j},$$

$$b_{mn}^{j} = \frac{j_n(m^j x^j)\left(x^j j_n(x^j)\right)' - j_n(x^j)\left(m^j x^j j_n(m^j x^j)\right)'}{j_n(m^j x^j)\left(x^j h_n^{(1)}(x^j)\right)' - h_n^{(1)}(x^j)\left(m^j x^j j_n(m^j x^j)\right)'} q_{mn}^{j}. \tag{2}$$

Here the superscript j indicates the particle number, a_{mn}^{j} and b_{mn}^{j} are scattering coefficients, p_{mn}^{j} and q_{mn}^{j} are incident coefficients, m^j is relative refractive index of the j-th particle, $x^j = kR^j$ is the size parameter, k is the wave number in surrounding medium, R^j is radius of the particle, j_n and $h_n^{(1)}$ are spherical Bessel and Hankel functions of the first kind. The field at the j-th particle is the sum of the external field and fields scattered by the other particles in the system:

$$p_{mn}^{j} = p_{mn}^{j,j} - \sum_{\substack{l=1 \\ l\neq j}}^{N} \sum_{\nu=1}^{\infty} \sum_{\mu=-\nu}^{\nu} \left(a_{\mu\nu}^{l} A_{mn}^{\mu\nu}(l,j) + b_{\mu\nu}^{l} B_{mn}^{\mu\nu}(l,j)\right),$$

$$q_{mn}^{j} = q_{mn}^{j,j} - \sum_{\substack{l=1 \\ l\neq j}}^{N} \sum_{\nu=1}^{\infty} \sum_{\mu=-\nu}^{\nu} \left(a_{\mu\nu}^{l} B_{mn}^{\mu\nu}(l,j) + b_{\mu\nu}^{l} A_{mn}^{\mu\nu}(l,j)\right). \tag{3}$$

Here $p_{mn}^{j,j}$, $q_{mn}^{j,j}$ are external field decomposition coefficients, $A_{mn}^{\mu\nu}(l,j)$, $B_{mn}^{\mu\nu}(l,j)$ are the translation coefficient [76]. Equations (2), (3) are the system of n linear algebraic equations. The solution of this system provides one with coefficients a_{mn}^{j}, b_{mn}^{j}, p_{mn}^{j}, q_{mn}^{j}.

Extinction and scattering cross-sections of n-th mode are defined as follows:

$$(C_{ext})_n = \frac{4\pi}{k^2} n(n+1)(2n+2) \sum_{j=1}^{N} \sum_{m=-n}^{n} \frac{(n-m)!}{(n+m)!} Re\left(p_{mn}^{j,j*} a_{mn}^{j} + q_{mn}^{j,j*} b_{mn}^{j}\right),$$

$$(C_{sca})_n = \frac{4\pi}{k^2} n(n+1)(2n+2) \sum_{j=1}^{N} \sum_{m=-n}^{n} \frac{(n-m)!}{(n+m)!} \left(|a_{mn}^{j}|^2 + |b_{mn}^{j}|^2\right). \tag{4}$$

The total cross section is the sum of cross-sections of all modes:

$$C_{ext} = \sum_{n=1}^{\infty} (C_{ext})_n, \quad C_{sca} = \sum_{n=1}^{\infty} (C_{sca})_n. \tag{5}$$

The absorption cross-section is

$$C_{abs} = C_{ext} - C_{sca}. \tag{6}$$

The efficiency of extinction in this paper is understood as the ratio of the extinction coefficient to the area of the unit cell of the periodic structure:

$$Q_{ext} = \frac{C_{ext}}{h^2}, \tag{7}$$

where h is a lattice period.

3. Results

3.1. Optical properties of a single aluminum sphere

Fig 2 a shows the extinction spectra of a single aluminum particle depending on its radius. It is seen that the increase of the particle radius results in increase of the number of resonances in the extinction spectrum, herewith their position is shifted to the long-wavelength range. Fig 2 b-g shows the decomposed extinction spectra of the single nanoparticles for different radii. As we can see each mode is located in different region in (R, λ) space, however they can overlap.

We should note that an increase in the particle radius leads to a sequential excitation of electric and magnetic modes. For example only electric dipole and quadrupole modes are excited in small particles. Octupole modes are excited in particles with radius over 50 nm. Besides that, the contribution of magnetic modes to extinction is much lower than the contribution of electric modes. In addition, these modes are excited in particles with radius over 80 nm. At the same time, as the order of multipole decomposition increases, both the electric and magnetic modes are excited at shorter wavelengths.

For comparison, the dipole extinction components of conventional plasmonic materials (Ag, Au) are shown in Fig. 3. One can

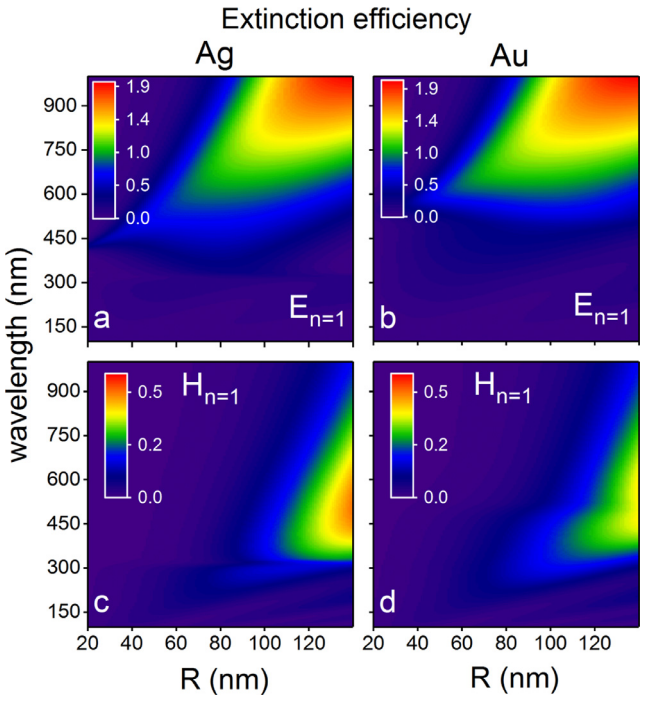

Fig. 3. The first order spherical multipoles components of extinction efficiency for single Ag and Au spherical nanoparticles of different radii R and wavelengths of incident light.

see in Figs 2 that extinction efficiency of magnetic dipole is two times lower than a one of corresponding electric dipole. However in Ag and Au the difference is more significant, by factor 5 and 7, respectively (see Fig. 3).

It is important to note that magnetic dipole modes in Ag and Au exist in particles with $R > 100$ nm, while in Al NPs the modes can be excited already at $R > 80$ nm. In this regard Aluminum seems to be more attractive in comparison with the conventional plasmonic materials, since the electric and magnetic modes can simultaneously be excited in particles of relatively smaller radius. We argue that this feature has a potential to be used for mode hybridization in periodic structures.

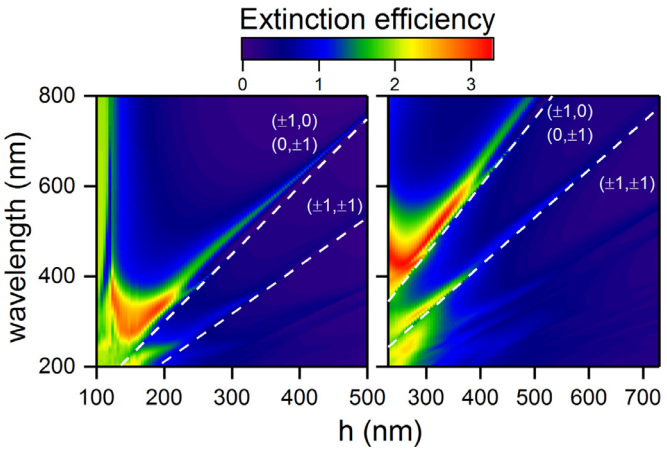

Fig. 4. Extinction efficiency of the Al nanoparticle array with different period h. The nanoparticle radius is $R = 60$ nm (left) and $R = 110$ nm (right), respectively.

3.2. Optical properties of a square array of aluminum spheres

Application of aluminum spherical nanoparticles as structural elements in 2D periodic arrays leads to a significant change in the extinction spectra. This is due to hybridization of the single particle modes with the collective modes of a lattice. Extinction spectra of periodic structures with different radii of the spherical nanoparticles and the periods of the lattice h are shown in Fig. 4. One can in these figure that the strong coupling between localized surface plasmon resonance and Wood-Rayleigh anomalies [2,3] leads to the emergence of high-quality collective resonances [77,78] with spectral positions close to the Wood-Rayleigh anomalies. Position of these anomalies for normal incidence of light for square arrays can be found with the following equation:

$$\lambda_{s,q} = h\sqrt{\frac{\varepsilon_m}{s^2+q^2}}, \tag{8}$$

where s, q are integers which represent the order of the phase difference in x and y directions. It should be noted that Eq. (8) describes the condition of constructive interference for particles within the YOZ plane [79]. Here and after λ is the vacuum wavelength. Different orders of the Wood-Rayleigh anomalies with (0,

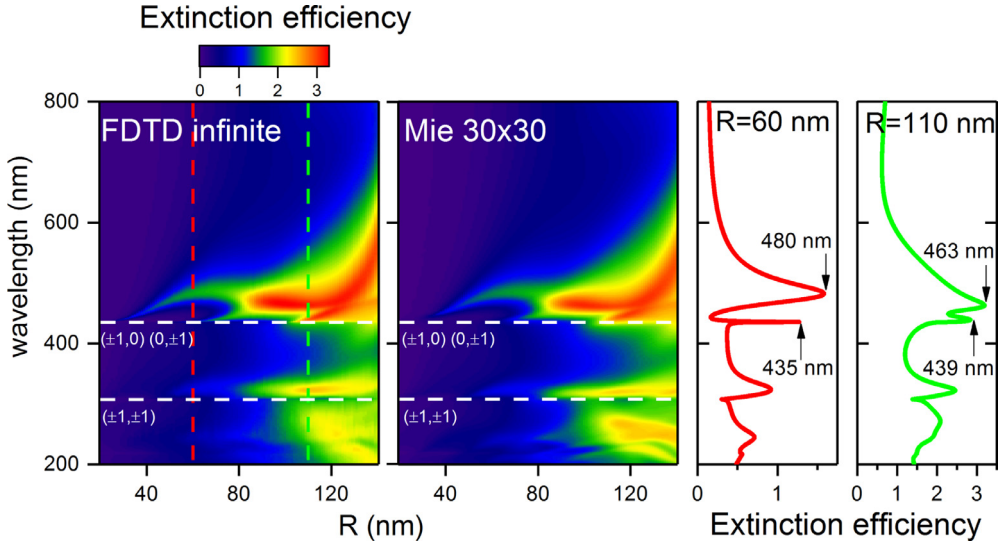

Fig. 5. Extinction spectra of the infinite (left) and 30 × 30 (right) arrays of Al NPs with $h = 290$ nm for different values of R calculated by FDTD and generalized Mie theory, respectively. White dashed line represent the different orders of the Rayleigh anomalies and white dots line represent the position of corresponding mode resonance.

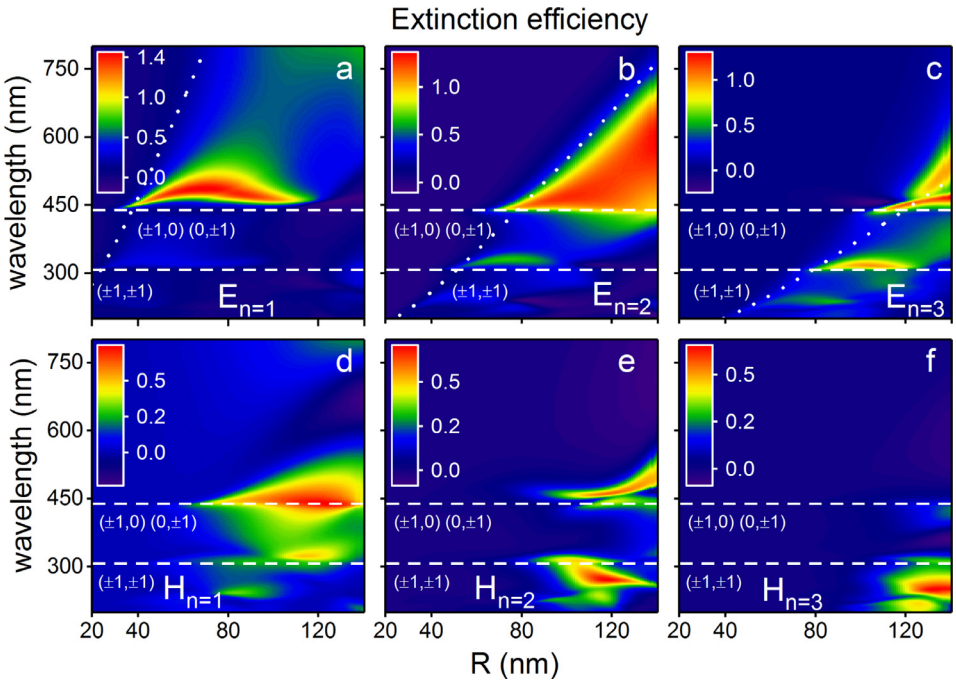

Fig. 6. Extinction efficiency decomposed in a set of spherical multipoles for square array consisting of Al NPs of different radii R and wavelengths of incidence light (a,b,c) are for the electrical field component while (d,e,f) are for magnetic field component. The array period is 290 nm. White dash lines represents the Rayleigh anomalies and white dots lines correspond to the electric field resonance condition in Eq. (2) when denominator of a_{mn}^{j} is equal to zero.

$\pm$ 1), ($\pm$ 1, 0) and ($\pm$ 1, $\pm$ 1) are shown in Fig. 4. Note, SLR in such structures can be tuned within the whole visible spectrum.

3.3. Finite size effects

Let us turn to the dependence of extinction spectra on the particle radius. Fig. 5 shows the extinction spectra of an infinite lattice with a period of $h = 290$ nm from aluminum nanospheres calculated by the FDTD method. To analyze the complex spectral pattern, we will use the generalized Mie theory, which will allow us to obtain the decomposition of extinction spectra by modes of spherical particles.

Note, that the generalized Mie theory allows us to calculate the optical properties of structures consisting of a finite number of particles. In this case, the extinction spectra of the 2D lattice can be modified by finite size effects (see [80]). Therefore, we have carried out comparative calculations of extinction spectra of an infinite periodic lattice and a lattice consisting of 30×30 particles. The calculation results are shown in Fig. 5.

The figure shows that the use of an array of particles 30×30 with a high degree accurately reproduces the spectral characteristics of the infinite lattice. It is important to note that good agreement is observed both for the wavelengths of the modes of 2D lattice and their amplitudes. Thus, we can use the generalized Mie theory to decompose the modes of a 2D lattice over spherical multipoles with minimal impact of the finite size effects on them. The results of the expansions are shown in Fig. 6.

White dots lines correspond to the electric field resonance condition in Eq. (2) when denominator of a_{mn}^{j} is equal to zero. We note that this equation is performed only for complex frequency. In this case the real part of frequency defines the position of the resonance while the imaginary part defines its line width. The spectral decomposition pattern is the result of the interaction of local resonances of single particles with the Rayleigh anomalies of the periodic array. For example, the electric field mode $E_{n=1}$ is excited in the particles with the radius over 40 nm, while $E_{n=2}$ is excited in the particles over 80 nm. Note that the excitation of $E_{n=3}$ is possible only in particles with minimum radius of about 120 nm.

An interesting fact is that the resonances of a single particle hybridize with the higher-order Rayleigh anomalies, which leads to a local increase in the extinction efficiency near the wavelengths corresponding to the position of the Rayleigh anomalies. A similar pattern is observed for the modes $E_{n=2}$ and $E_{n=3}$, while for the mode $E_{n=3}$ there is no increase in the extinction efficiency in the vicinity of the second Rayleigh anomaly with a wavelength of 300 nm. This behavior can be explained by the extinction efficiencies of single particle (Fig. 2). So for the $E_{n=1}$ mode, the Rayleigh anomaly crosses only the edge of the resonance region, while for $E_{n=2}$ and $E_{n=3}$ it crosses the range with high extinction efficiency.

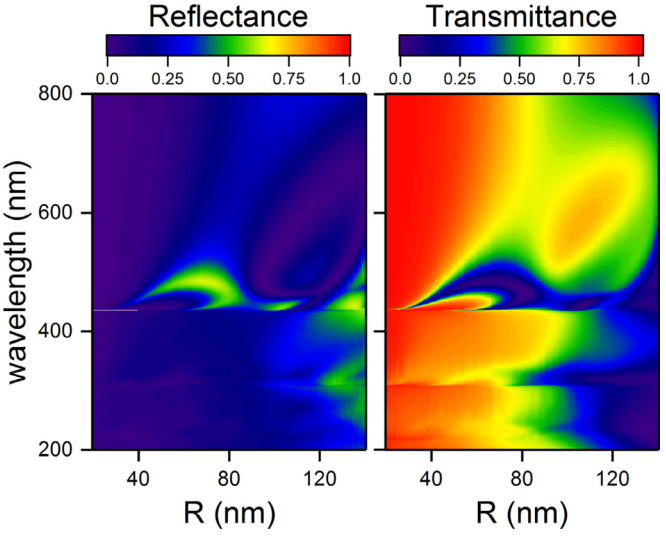

Fig. 7. Reflectance and transmittance of the Al nanoparticle array with different radii R. The array period is $h = 290$ nm.

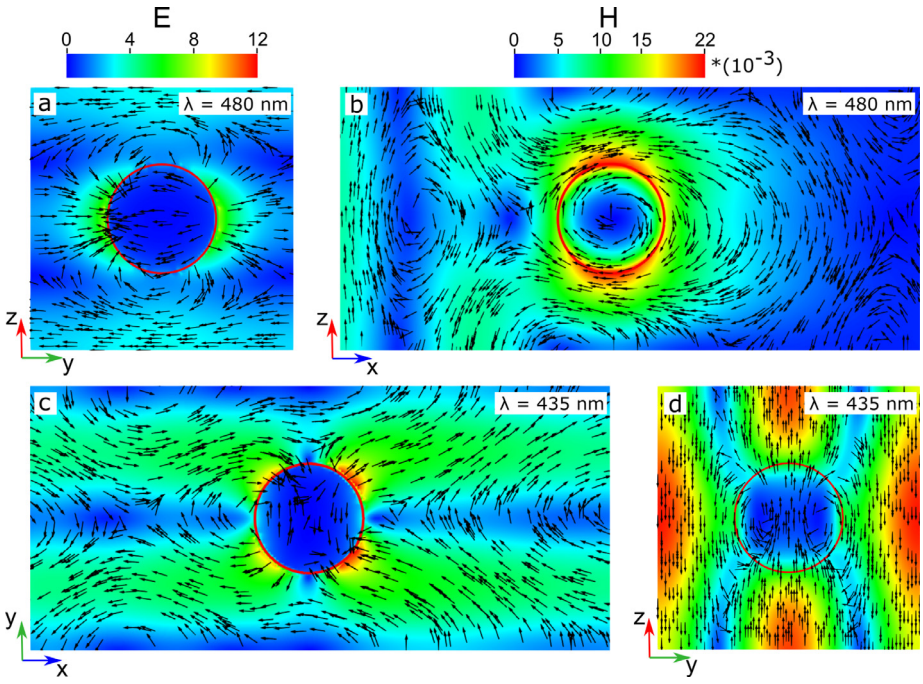

Fig. 8. The configuration of electric (a,c) and magnetic (b,d) fields at 435 and 480 nm, respectively for $R = 60$ nm and $h = 290$ nm.

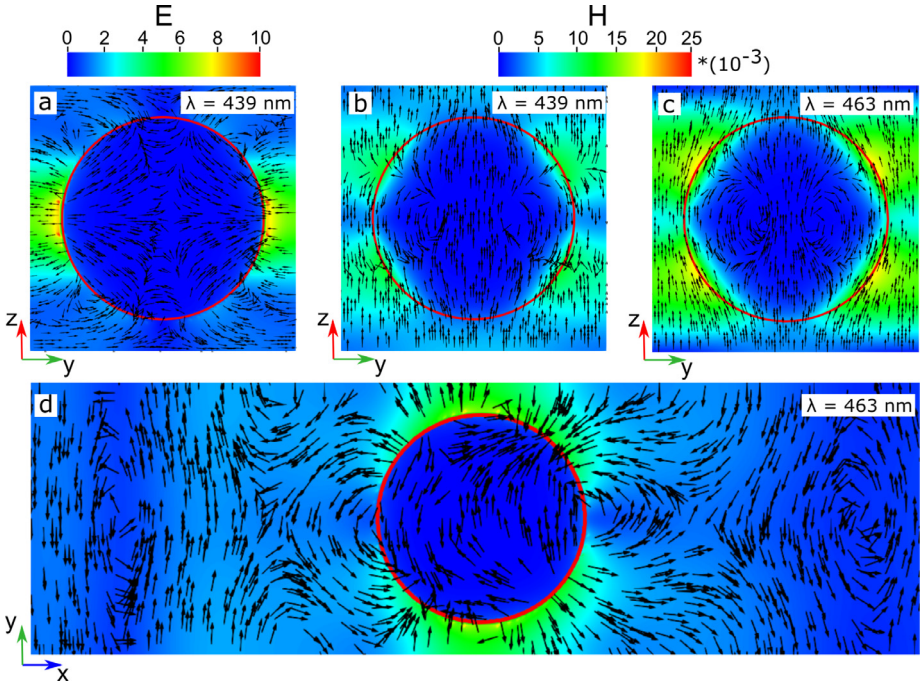

Fig. 9. The configuration of electric (a,d) and magnetic (b,c) fields at 439 and 463 nm, respectively for $R = 110$ nm and $h = 290$ nm.

Fig. 7 shows the transmittance and reflectance spectra of the array structure calculated by the FDTD method. One can see that the structure reflects radiation only in the spectral range of the hybrid resonance modes. Thus, tuning of the spectra can be efficiently performed by variation of the lattice period and nanoparticle sizes. Importantly, that for small particles ($R < 40$ nm) the transmittance of the structure is about 100%. But for large particles ($R > 120$ nm) the structure is not transparent in whole spectral range. Note, that the reflection is measured by monitor located before the source of a plane wave, while the transmission measured by monitor located inside TFSF after the structure. In this case the transmission monitor detects the total field. In addition, we note an important methodological aspect. The coupled dipole approximation (CDA) [81] is a popular method in computational electrodynamics being widely used for studying of periodical structures due to its simplicity and ability to simulate the structures consisting of large number of particles. Note, that for the structures considered in this paper this method can be applied only to the particles with small radius. This is due to the fact that in this case only electro- and magneto-dipole modes are excited in the nanoparticles. But in practice an increase of the nanoparticle size results in an abrupt growth of the contribution of higher or-

der modes. Fig. 6 shows that these modes are limited, on one side, by the Rayleigh anomaly, and, on another side, by the resonance condition in Eq. (2). In this way, the Mie theory allows one to find the limits of the CDA method applicability, which can be useful in the study of structures with a large number of particles.

4. Resonant field configuration

Now let us turn to the field configurations that correspond to the extinction maxima. For $R = 60$ nm the maximum extinction is achieved at the wavelength 435 nm and 480 nm while for $R = 110$ nm at 439 nm and 463 nm (see Fig. 5). The corresponding field pattern for individual particle in the lattice are shown in Figs. 8 and 9.

As can be seen that at the wavelength of 480 nm the configuration of the electric and magnetic fields corresponds to the electric dipole. While at a wavelength of 435 nm the field configuration resemble the combination of an electric quadrupole and a magnetic dipole. Note that the electric dipole is excited in the plane of incident wave, and the quadrupole is in the plane of light polarization. A more complex configuration of the electric field is observed at a wavelength of 439 nm. It is seen in Fig. 9 that in this case the third order mode is formed and it has three pairs of antisymmetric poles while modes of the second order are formed at the wavelength of 463 nm Fig. 9d. Note that both at the wavelength of 439 nm and at the wavelength of 463 nm, the configuration of magnetic fields resembles the magnetic dipole.

For particles with a radius of 110 nm and a wavelength of incident light of 448 nm, magnetic modes of only the first order can be excited in such media, while a change in the wavelength up to 458 nm leads to the excitation of magnetic modes of the second order. The obtained field distributions are in full agreement with the results of the decomposition of the extinction spectra received by the generalized Mie theory. Thus, the variation of the lattice parameters and the wavelength of the incident light makes it possible to control the modes of 2D periodic lattices.

5. Conclusion

To conclude, the extinction spectra of the single aluminium nanoparticles and nanoparticle arrays vs the particle radius have been investigated. It was shown that for single nanoparticles an increase of their radius leads to a sequential excitation and decay of electric and magnetic modes. We note that the modes of a single particle do not interact with each other.

However, the different scenario is observed for the nanoparticle array. In this case the different orders of the particle modes interact with each other and with the Rayleigh anomalies that results in formation of hybrid modes. The spectral manifestations of hybrid modes are the formation of narrow lines in the extinction spectra and the corresponding hybrid configurations of the electromagnetic field.

The feature here is that the each mode of both electric and magnetic fields interact with the Rayleigh anomalies of different orders. As the result we observe the increased extinction efficiency in the vicinity of the Rayleigh anomalies. This effect can be used to control the spectral position of the extinction maximum.

Thus, obtaining the physical insight into the nature of the mode coupling in the Al nanoparticle arrays paves a way for efficient control of their optical response in various photonic applications, primarily in the short-wavelength spectral range, which can not be easily achieved with other alternative strategies.

Funding

The reported study was funded by the grant of the President of Russian Federation (agreement 075-15-2019-676); the Russian Foundation for Basic Research, Government of Krasnoyarsk Territory, Krasnoyarsk Regional Fund of Science (Grant No.18-42-240013); the State contract with Siberian Federal University for scientific research; Russian Science Foundation project number 19-72-00066 (investigation of finite size effects).

Author statement

Valeriy S. Gerasimov and Rashid G. Bikbaev performed the calculations, visualized the results and drafted the manuscript. Alexander E. Ershov developed software, methods and analytical expressions, Sergey V. Karpov and Sergey P. Polyutov supervised the whole study and finalized the manuscript.

Declaration of Competing Interest

The authors declare that they have no known competing financial interests or personal relationships that could have appeared to influence the work reported in this paper.

Acknowledgement

We thank Dr. I. Rasskazov and Dr. P. Semina for fruitful and valuable discussions.

References

[1] Evlyukhin AB, Reinhardt C, Zywietz U, Chichkov BN. Collective resonances in metal nanoparticle arrays with dipole-quadrupole interactions. Phys Rev B 2012;85(24):245411. doi:10.1103/PhysRevB.85.245411.
[2] Rayleigh L. On the dynamical theory of gratings. Proc R Soc A 1907;79(532):399–416. doi:10.1098/rspa.1907.0051.
[3] Wood RW. On a remarkable case of uneven distribution of light in a diffraction grating spectrum. Proceedings of the Physical Society of London 1902;18(1):269–75. doi:10.1088/1478-7814/18/1/325. http://stacks.iop.org/1478-7814/18/i=1/a=325?key=crossref.7ebbe1383fb00dffe4b52e1569cdd953
[4] Zou S, Schatz GC. Narrow plasmonic/photonic extinction and scattering line shapes for one and two dimensional silver nanoparticle arrays. J Chem Phys 2004;121(24):12606–12. doi:10.1063/1.1826036.
[5] Zou S, Janel N, Schatz GC. Silver nanoparticle array structures that produce remarkably narrow plasmon lineshapes. J Chem Phys 2004;120(23):10871–5. doi:10.1063/1.1760740.
[6] Markel VA. Divergence of dipole sums and the nature of non-Lorentzian exponentially narrow resonances in one-dimensional periodic arrays of nanospheres. J Phys B 2005;38(7):L115–21. doi:10.1088/0953-4075/38/7/L02.
[7] Auguié B, Barnes WL. Collective resonances in gold nanoparticle arrays. Phys Rev Lett 2008;101(14):143902. doi:10.1103/PhysRevLett.101.143902.
[8] Kravets VG, Schedin F, Grigorenko AN. Extremely narrow plasmon resonances based on diffraction coupling of localized plasmons in arrays of metallic nanoparticles. Phys Rev Lett 2008;101(8):87403. doi:10.1103/PhysRevLett.101.087403.
[9] Chu Y, Schonbrun E, Yang T, Crozier KB. Experimental observation of narrow surface plasmon resonances in gold nanoparticle arrays. Appl Phys Lett 2008;93(18):181108. doi:10.1063/1.3012365.
[10] Khlopin D, Laux F, Wardley WP, Martin J, Wurtz GA, Plain J, et al. Lattice modes and plasmonic linewidth engineering in gold and aluminum nanoparticle arrays. J Opt Soc Am B 2017;34(3):691–700. doi:10.1364/JOSAB.34.000691.
[11] Utyushev AD, Isaev IL, Gerasimov VS, Ershov AE, Zakomirnyi VI, Rasskazov IL, et al. Engineering novel tunable optical high-q nanoparticle array filters for a wide range of wavelengths. Opt Express 2020;28(2):1426. doi:10.1364/oe.28.001426.
[12] Zhang Z-S, Yang Z-J, Li J-B, Hao Z-H, Wang Q-Q. Plasmonic interferences in two-dimensional stacked double-disk array. Appl Phys Lett 2011;98(17):173111. doi:10.1063/1.3583999.
[13] Lin L, Yi Y. Orthogonal and parallel lattice plasmon resonance in core-shell SiO_2/au nanocylinder arrays. Opt Express 2015;23(1):130. doi:10.1364/OE.23.000130.
[14] Humphrey AD, Meinzer N, Starkey TA, Barnes WL. Surface lattice resonances in plasmonic arrays of asymmetric disc dimers. ACS Photon 2016;3(4):634–9. doi:10.1021/acsphotonics.5b00727.
[15] Mahi N, Lévêque G, Saison O, Marae-Djouda J, Caputo R, Gontier A, et al. In depth investigation of lattice plasmon modes in substrate-supported gratings of metal monomers and dimers. J Phys Chem C 2017;121(4):2388–401. doi:10.1021/acs.jpcc.6b11321.
[16] Grigoriev V, Varault S, Boudarham G, Stout B, Wenger J, Bonod N. Singular analysis of fano resonances in plasmonic nanostructures. Phys Rev A 2013;88(6):63805. doi:10.1103/PhysRevA.88.063805.

[17] Wang D, Yang A, Hryn AJ, Schatz GC, Odom TW. Superlattice plasmons in hierarchical au nanoparticle arrays. ACS Photon 2015;2(12):1789–94. doi:10.1021/acsphotonics.5b00546.

[18] Nicolas R, Lévêque G, Marae-Djouda J, Montay G, Madi Y, Plain J, et al. Plasmonic mode interferences and fano resonances in metal-Insulator- Metal nanostructured interface. Sci Rep 2015;5(1):14419. doi:10.1038/srep14419.

[19] Guo R, Hakala TK, Törmä P. Geometry dependence of surface lattice resonances in plasmonic nanoparticle arrays. Phys Rev B 2017;95(15):155423. doi:10.1103/PhysRevB.95.155423.

[20] Gerasimov V, Ershov A, Bikbaev R, Rasskazov I, Timofeev I, Polyutov S, et al. Engineering mode hybridization in regular arrays of plasmonic nanoparticles embedded in 1D photonic crystal. Journal of Quantitative Spectroscopy and Radiative Transfer 2019;224:303–8. doi:10.1016/j.jqsrt.2018.11.028. https://linkinghub.elsevier.com/retrieve/pii/S0022407318306149

[21] Adato R, Yanik AA, Amsden JJ, Kaplan DL, Omenetto FG, Hong MK, et al. Ultra-sensitive vibrational spectroscopy of protein monolayers with plasmonic nanoantenna arrays. Proc Natl Acad Sci 2009;106(46):19227–32. doi:10.1073/pnas.0907459106.

[22] Li Z, Butun S, Aydin K. Ultranarrow band absorbers based on surface lattice resonances in nanostructured metal surfaces. ACS Nano 2014;8(8):8242–8. doi:10.1021/nn502617t.

[23] Thackray BD, Kravets VG, Schedin F, Auton G, Thomas PA, Grigorenko AN. Narrow collective plasmon resonances in nanostructure arrays observed at normal light incidence for simplified sensing in asymmetric air and water environments. ACS Photon 2014;1(11):1116–26. doi:10.1021/ph5002186.

[24] Gutha RR, Sadeghi SM, Wing WJ. Ultrahigh refractive index sensitivity and tunable polarization switching via infrared plasmonic lattice modes. Appl Phys Lett 2017;110(15):153103. doi:10.1063/1.4980060.

[25] Zhou W, Dridi M, Suh JY, Kim CH, Co DT, Wasielewski MR, et al. Lasing action in strongly coupled plasmonic nanocavity arrays. Nat Nanotechnol 2013;8(7):506–11. doi:10.1038/nnano.2013.99.

[26] Vecchi G, Giannini V, Gómez Rivas J. Shaping the fluorescent emission by lattice resonances in plasmonic crystals of nanoantennas. Phys Rev Lett 2009;102(14):146807. doi:10.1103/PhysRevLett.102.146807.

[27] Laux F, Bonod N, Gérard D. Single emitter fluorescence enhancement with surface lattice resonances. J Phys Chem C 2017;121(24):13280–9. doi:10.1021/acs.jpcc.7b04207.

[28] Lin J-Y, Zhong K-D, Lee P-T. Plasmonic behaviors of metallic AZO thin film and AZO nanodisk array. Opt Express 2016;24(5):5125. doi:10.1364/oe.24.005125.

[29] Zakomirnyi VI, Rasskazov IL, Gerasimov VS, Ershov AE, Polyutov SP, Karpov SV. Refractory titanium nitride two-dimensional structures with extremely narrow surface lattice resonances at telecommunication wavelengths. Appl Phys Lett 2017;111(12):123107. doi:10.1063/1.5000726.

[30] Knight MW, King NS, Liu L, Everitt HO, Nordlander P, Halas NJ. Aluminum for plasmonics. ACS Nano 2014;8(1):834–40. doi:10.1021/nn405495q.

[31] Gérard D, Gray SK. Aluminium plasmonics. Journal of Physics D: Applied Physics 2015;48(18):184001. doi:10.1088/0022-3727/48/18/184001. http://stacks.iop.org/0022-3727/48/i=18/a=184001?key=crossref.47c09902307b4ae6359f47bdee49e952

[32] Geddes CD, Lakowicz JR. Editorial: metal-Enhanced fluorescence. J Fluoresc 2002;12(2):121–9. doi:10.1023/A:1016875709579.

[33] Lakowicz JR. Radiative decay engineering 5: metal-enhanced fluorescence and plasmon emission. Analytical Biochemistry 2005;337(2):171–94. doi:10.1016/j.ab.2004.11.026. http://www.sciencedirect.com/science/article/pii/S0003269704009303

[34] Fort E, Grésillon S. Surface enhanced fluorescence. J Phys D Appl Phys 2007;41(1):13001. doi:10.1088/0022-3727/41/1/013001.

[35] Tan SJ, Zhang L, Zhu D, Goh XM, Wang YM, Kumar K, et al. Plasmonic color palettes for photorealistic printing with aluminum nanostructures. Nano Lett 2014;14(7):4023–9. doi:10.1021/nl501460x.

[36] Fouladi Mahani F, Mokhtari A, Mehran M. Design and development of aluminum nanoring arrays for realization of dual-mode operation plasmonic color filters. J Opt Soc Am B 2018;35(8):1764. doi:10.1364/JOSAB.35.001764.

[37] Song M, Kudyshev ZA, Yu H, Boltasseva A, Shalaev VM, Kildishev AV. Achieving full-color generation with polarization-tunable perfect light absorption. Opt Mater Express 2019;9(2):779. doi:10.1364/OME.9.000779.

[38] Kochergin V, Neely L, Jao C-Y, Robinson HD. Aluminum plasmonic nanostructures for improved absorption in organic photovoltaic devices. Appl Phys Lett 2011;98(13):133305. doi:10.1063/1.3574091.

[39] Uhrenfeldt C, Villesen TF, Têtu A, Johansen B, Larsen AN. Broadband photocurrent enhancement and light-trapping in thin film si solar cells with periodic al nanoparticle arrays on the front. Opt Express 2015;23(11):A525–38. doi:10.1364/OE.23.00A525.

[40] Zhang D, Yang X, Hong X, Liu Y, Feng J. Aluminum nanoparticles enhanced light absorption in silicon solar cell by surface plasmon resonance. Opt Quantum Electron 2015;47(6):1421–7. doi:10.1007/s11082-014-0103-0.

[41] Zhan Y, Cai B, Jia B. Ultraviolet plasmonic aluminium nanoparticles for highly efficient light incoupling on silicon solar cells. Nanomaterials 2016;6(6). doi:10.3390/nano6060095.

[42] Wiecha PR, Mennemanteuil M-M, Khlopin D, Martin J, Arbouet A, Gérard D, et al. Local field enhancement and thermoplasmonics in multimodal aluminum structures. Phys Rev B 2017;96(3):035440. doi:10.1103/PhysRevB.96.035440.

[43] Zhang Y, Shi L, Hu D, Chen S, Xie S, Lu Y, et al. Full-visible multifunctional aluminium metasurfaces by in situ anisotropic thermoplasmonic laser printing. Nanoscale Horiz 2019;4(3):601–9. doi:10.1039/C9NH00003H.

[44] Ekinci Y, Solak HH, Löffler JF. Plasmon resonances of aluminum nanoparticles and nanorods. J Appl Phys 2008;104(8). doi:10.1063/1.2999370.

[45] Langhammer C, Schwind M, Kasemo B, Zorić I. Localized surface plasmon resonances in aluminum nanodisks. Nano Lett 2008;8(5):1461–71. doi:10.1021/nl080453i.

[46] Maidecchi G, Gonella G, Proietti Zaccaria R, Moroni R, Anghinolfi L, Giglia A, et al. Deep ultraviolet plasmon resonance in aluminum nanoparticle arrays. ACS Nano 2013;7(7):5834–41. doi:10.1021/nn400918n.

[47] Campos A, Arbouet A, Martin J, Gérard D, Proust J, Plain J, et al. Plasmonic breathing and edge modes in aluminum nanotriangles. ACS Photon 2017;4(5):1257–63. doi:10.1021/acsphotonics.7b00204.

[48] Clark BD, Jacobson CR, Lou M, Yang J, Zhou L, Gottheim S, et al. Aluminum nanorods. Nano Lett 2018;18(2):1234–40. doi:10.1021/acs.nanolett.7b04820.

[49] Pathak NK, Parthasarathi P, Kumar PS, Sharma RP. Tuning of the surface plasmon resonance of aluminum nanoshell near-infrared regimes. Phys. Chem. Chem. Phys. 2019;21(18):9441–9. doi:10.1039/C9CP01115C.

[50] Clark BD, Jacobson CR, Lou M, Renard D, Wu G, Bursi L, et al. Aluminum Nanocubes Have Sharp Corners. ACS Nano 2019. doi:10.1021/acsnano.9b05277. acsnano.9b05277

[51] Ross MB, Schatz GC. Aluminum and indium plasmonic nanoantennas in the ultraviolet. J Phys Chem C 2014;118(23):12506–14. doi:10.1021/jp503323u.

[52] Flauraud V, Bernasconi GD, Butet J, Alexander DTL, Martin OJF, Brugger J. Mode coupling in plasmonic heterodimers probed with electron energy loss spectroscopy. ACS Nano 2017;11(4):3485–95. doi:10.1021/acsnano.6b08589.

[53] Kannegulla A, Liu Y, Wu B, Cheng L-J. Aluminum ultraviolet-visible plasmonic arrays for broadband and wavelength-selective enhancements of quantum dot emission. Appl Phys Lett 2017;111(8). doi:10.1063/1.4986970.

[54] Yang A, Hryn AJ, Bourgeois MR, Lee W-K, Hu J, Schatz GC, et al. Programmable and reversible plasmon mode engineering. Proc Natl Acad Sci 2016;113(50):14201–6. doi:10.1073/pnas.1615281113.

[55] Tseng ML, Yang J, Semmlinger M, Zhang C, Nordlander P, Halas NJ. Two-dimensional active tuning of an aluminum plasmonic array for full-Spectrum response. Nano Lett 2017;17(10):6034–9. doi:10.1021/acs.nanolett.7b02350.

[56] Huttunen MJ, Reshef O, Stolt T, Dolgaleva K, Boyd RW, Kauranen M. Efficient nonlinear metasurfaces by using multiresonant high-Q plasmonic arrays. J Opt Soc Am B 2019;36(7):E30. doi:10.1364/JOSAB.36.000E30.

[57] Knudson MP, Li R, Wang D, Wang W, Schaller RD, Odom TW. Polarization-dependent lasing behavior from low-Symmetry nanocavity arrays. ACS Nano 2019;13(7):7435–41. doi:10.1021/acsnano.9b01142.

[58] Li R, Bourgeois MR, Cherqui C, Guan J, Wang D, Hu J, et al. Hierarchical Hybridization in Plasmonic Honeycomb Lattices. Nano Letters 2019;17. doi:10.1021/acs.nanolett.9b02661. acs.nanolett.9b02661

[59] Li R, Wang D, Guan J, Wang W, Ao X, Schatz GC, et al. Plasmon nanolasing with aluminum nanoparticle arrays [Invited]. J Opt Soc Am B 2019;36(7):E104–11. doi:10.1364/JOSAB.36.00E104.

[60] Murai S, Saito M, Kawachiya Y, Ishii S, Nakanishi T, Tanaka K. Temperature sensing of a plasmonic nanocylinder array by a polymer film containing chameleon complex. J Opt Soc Am B 2019;36(7):E15–20. doi:10.1364/JOSAB.36.000E15.

[61] Lozano G, Louwers DJ, Rodríguez SR, Murai S, Jansen OT, Verschuuren MA, et al. Plasmonics for solid-state lighting: enhanced excitation and directional emission of highly efficient light sources. Light: Sci Appl 2013;2(5). doi:10.1038/lsa.2013.22. e66–e66

[62] Kawachiya Y, Murai S, Saito M, Sakamoto H, Fujita K, Tanaka K. Collective plasmonic modes excited in al nanocylinder arrays in the UV spectral region. Opt Express 2018;26(5):5970. doi:10.1364/OE.26.005970.

[63] Kawachiya Y, Murai S, Saito M, Fujita K, Tanaka K. Photoluminescence decay rate of an emitter layer on an al nanocylinder array: effect of layer thickness. J Opt Soc Am B 2019;36(7):E1–8. doi:10.1364/josab.36.0000e1.

[64] Rodriguez SRK, Arango FB, Steinbusch TP, Verschuuren MA, Koenderink AF, Rivas JG. Breaking the symmetry of forward-Backward light emission with localized and collective magnetoelectric resonances in arrays of pyramid-Shaped aluminum nanoparticles. Phys Rev Lett 2014;113(24):247401. doi:10.1103/PhysRevLett.113.247401.

[65] Murai S, Kawachiya Y, Tanaka K. Confinement of ultraviolet light using lattice modes in Al and Si nanocylinder arrays. Opt Mater Express 2019;9(8):3310. doi:10.1364/OME.9.003310.

[66] Todisco F, Esposito M, Panaro S, De Giorgi M, Dominici L, Ballarini D, et al. Toward cavity quantum electrodynamics with hybrid photon gap-plasmon states. ACS Nano 2016;10(12):11360–8. doi:10.1021/acsnano.6b06611.

[67] Fu X, Ren F-F, Sun S, Tian Y, Wu Y, Lou P, et al. High-sensitivity nanostructured aluminium ultrathin film sensors with spectral response from ultraviolet to near-infrared. Phys Scr 2019;94(5):55504. doi:10.1088/1402-4896/ab0a12.

[68] Martin J, Kociak M, Mahfoud Z, Proust J, Gérard D, Plain J. High-resolution imaging and spectroscopy of multipolar plasmonic resonances in aluminum nanoantennas. Nano Lett 2014;14(10):5517–23. doi:10.1021/nl501850m.

[69] Martin J, Proust J, Gérard D, Plain J. Localized surface plasmon resonances in the ultraviolet from large scale nanostructured aluminum films. Opt Mater Express 2013;3(7):954. doi:10.1364/OME.3.000954.

[70] Zhang F, Proust J, Gérard D, Plain J, Martin J. Reduction of plasmon damping in aluminum nanoparticles with rapid thermal annealing. J Phys Chem C 2017;121(13):7429–34. doi:10.1021/acs.jpcc.7b00909.

[71] Smith D, Shiles E, Inokuti M. The optical properties of metallic aluminum. In: Palik ED, editor. Handbook of optical constants of solids. Burlington: Academic Press; 1997. p. 369–406. doi:10.1016/B978-012544415-6.50016-9.

[72] Markel VA. What is extinction? operational definition of the extinguished power for plane waves and collimated beams. J Quant Spectrosc Radiat Transfer 2020;246:106933. doi:10.1016/j.jqsrt.2020.106933.
[73] Lumerical Solutions, "FDTD Solutions". www.lumerical.com/tcad-products/fdtd/.
[74] Potter M, Bérenger J-P. A review of the total field/scattered field technique for the FDTD method. FERMAT 2017;19:1.
[75] Mie G. Beiträge zur optik trüber medien, speziell kolloidaler metallösungen. Ann Phys 1908;330(3):377–445. doi:10.1002/andp.19083300302.
[76] Xu Y-l. Electromagnetic scattering by an aggregate of spheres. Appl Opt 1995;34(21):4573. doi:10.1364/AO.34.004573.
[77] Ross MB, Mirkin CA, Schatz GC. Optical properties of one-, two-, and three-dimensional arrays of plasmonic nanostructures. J Phys Chem C 2016;120(2):816–30. doi:10.1021/acs.jpcc.5b10800.
[78] Kravets VG, Kabashin AV, Barnes WL, Grigorenko AN. Plasmonic surface lattice resonances: a review of properties and applications. Chem Rev 2018;118(12):5912–51. doi:10.1021/acs.chemrev.8b00243.
[79] Bonod N, Neauport J. Diffraction gratings: from principles to applications in high-intensity lasers. Adv Opt Photonics 2016;8(1):156–99. doi:10.1364/AOP.8.000156.
[80] Zakomirnyi VI, Ershov AE, Gerasimov VS, Karpov SV, Ågren H, Rasskazov IL. Collective lattice resonances in arrays of dielectric nanoparticles: a matter of size. Opt Lett 2019;44(23):5743. doi:10.1364/ol.44.005743.
[81] Markel V. Coupled-dipole approach to scattering of light from a one-dimensional periodic dipole structure. J Mod Opt 1993;40(11):2281–91. doi:10.1080/09500349314552291.